Dehydroacetic Acid-Phenylhydrazone as a Potential Inhibitor for Wild-Type HIV-1 Protease: Structural, DFT, Molecular Dynamics, 3D QSAR and ADMET Characteristics

Ibeji, Collins Ugochukwu*+●

Catalysis and Peptide Research Unit, School of Health Sciences, University of KwaZulu-Natal, Durban 4041, SOUTH AFRICA

Ujam, Oguejiofo Theophilus

Department of Pure and Industrial Chemistry, University of Nigeria, Nsukka, 410001, Enugu State, NIGERIA

Chukwuma Chime, Charles

Department of Industrial Chemistry, Enugu State University of Science and Technology Enugu, State, NIGERIA

Akpomie, Kovo Godfrey

Department of Pure and Industrial Chemistry, University of Nigeria, Nsukka, 410001, Enugu State, NIGERIA

Anarado, Chigozie John Onyinye

Department of Pure and Industrial Chemistry, Nnamdi Azikiwe University, P.M.B 5025, Awka, Anambra State, NIGERIA

Odewole, Olufemi Abiola

Department of Pure and Industrial Chemistry, University of Nigeria, Nsukka, 410001, Enugu State, NIGERIA

Grishina, Maria; Potemkin, Valdimir

South Ural State University, Laboratory of Computational Modelling of Drugs, Tchaikovsky Str. 20-A, Chelyabinsk, RUSSIA

ABSTRACT: *Despite several studies towards anti-HIV therapy, HIV infections remain a challenge due to the resistivity of developed drugs. The emergence of new HIV-1 PR mutations has led to the drug resistance of the available FDA-approved drugs and lower activity towards the HIV protease. Based on this the molecular properties of 4-hydroxy-6-methyl-3-[(1E)-1-(2-phenylhydrazinylidene) ethyl]-2H-pyran-2-one (DHAA-PH) has been carried out using the hybrid Density Functional Theory (DFT) and Time-Dependent (TDFT) method at B3LYP/6-31+G(d,p) levels of theory. To substantiate the sensitivity of functional applied M06-2X/ 6-31 1++G(2d,2p) and mPWB1W/6-311++G(2d,2p) was used to calculate the geometric, IR, ^{1}H NMR, and energy gap calculations. DFT calculations*

with M06-2X and mPWB1W were observed to agree with the experiment compared to B3LYP functional. The absorption spectra of DHAA-PH showed three distinct bands which were designated as S_0 to S_1, S_0 to S_2, and S_0 to S_3 in order of increasing energy. The high intensity (oscillator strength) of S_0 to S_1 infers that the transition is quantum-mechanically allowed, while the low intensity of S_0 to S_2 and S_0 to S_3 transitions suggests quantum mechanically forbidden transitions. Molecular dynamics simulations revealed that the obtained MMGBSA binding energies are better compared to the experimentally reported binding energies for HIV-1 protease inhibitors. 3D QSAR and computational ADMET study were performed. Pharmacophore fragments of the compound were identified as well as the fragments determining its toxicity and metabolic properties. Based on the analysis of these fragments, the ways to further design promising HIV1-protease inhibitors were proposed.

INTRODUCTION

Human Immunodeficiency Viruses (HIV) has been rated one of the predominant cause of death in many countries [1]. One of the most prominent and studied targets against HIV is HIV-1 protease [2]. The effortlessness transfer of the virus and drug resistivity have geared up the burden for the search for new and promising anti-HIV drugs [3, 4]. To combat this, synthesis of HIV protease potential inhibitors have been the goal of much research [4]. HIV protease structural conformation is a C_2-symmetric homodimer of 99 amino monomers with substrate binding pockets [5, 6] with the active-active site composed of catalytic residue ASP25 and ASP25' [7]. Synthesized compound mimics the active sites and binds to the active sites of the protein. The main interaction is with the carboxylic groups of the catalytic aspartic acid residues of the enzyme [8] and in general, compounds that form more hydrogen bonds with the active site, display improved activity [9-11]. Pyran-2-one and its derivatives have been a subject of study because they serve as building blocks for complex compounds due to its unsaturated cyclic nature [12]. Its derivatives are essential group of compounds with quite interesting applications [13, 14]. Their metal complexes have found applications as therapeutic agents against bacteria based on selective DNA cleavage ability [15]. Our group reported the synthesis, NMR and X-ray structural characterization of 4-hydroxy-6-methyl -3-[(1*E*)-1-(2-phenylhydrazinylidene)ethyl]-2*H*-pyran-2-one (DHAA-PH) [16], Scheme 1, but no theoretical calculations have been done on this compound to provide information on possible interaction, dynamics and its inhibitory potential activity against wild-type HIV-1 protease. Binding

free energy calculations is an essential study in structure-based drug design [17-19] which has been reported to be good in the design of HIV protease inhibitors [18]. These can be obtained using several methods such as Free Energy Perturbation (FEP) [20, 21], and molecular mechanics generalized Born (GB) Surface Area (MM-GBSA) and Poison-Boltzmann surface area (MM-PBSA) [22, 23]. MM-GBSA has been widely used for protein-drugs [24], nucleic acid [25] and ligand binding interaction [26, 27]. This approach has been reported to be one of the best models for predicting relative binding free energies of proteins due to its accuracy especially for ranking the binding affinities of the inhibitors[28, 29].

In this study, the structural, molecular properties, and the binding potential of DHAA-PH against wild-type HIV 1 protease was examined using quantum mechanics methods, molecular dynamics simulations and QSAR study along with elucidation of ADMET characteristics.

COMPUTATIONAL METHODS

Quantum mechanics calculations

DHAA-PH was optimized in gas phase and in DMSO as the solvent, using the hybrid Density Functional Theory (DFT) method at B3LYP/6-31+G(d,p) levels of theory, which is the combination of functional hybrid exchange of Becke's three, [30] with functional correlation gradient of *Lee* and *Yang* [31]. Properties such as the geometric properties; selected bond length, the electronic properties; dipole moments, energy gap, and IR was calculated using DFT-B3LYP/6-31+G(d,p) levels of theory and the frequency calculations were performed with a scaling factor of 0.964[32]. The excitation energy, absorption
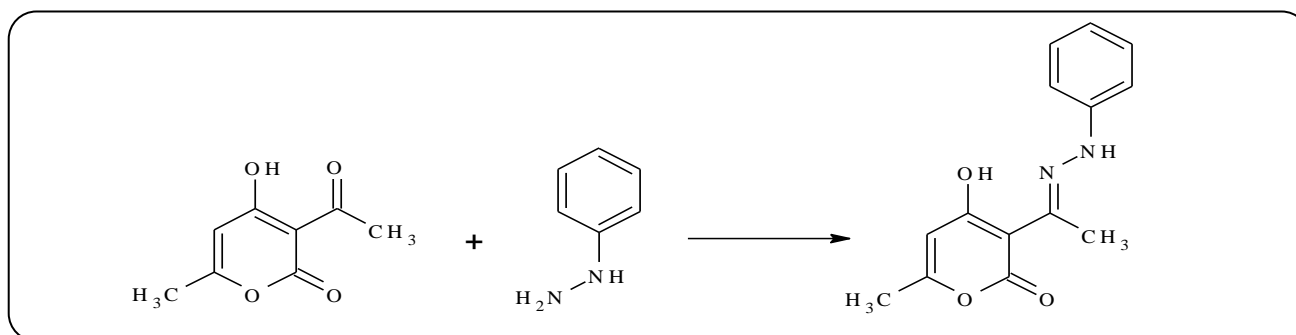
Scheme 1: The synthetic scheme of DHAA-PH [16].

maxima and oscillator strength were calculated using Time Dependent Density Functional Theory (TDDFT) method at B3LYP/6-31+G(d,p).

[1]H magnetic shielding constants, obtained on a δ-scale, relative to the TMS (reference) was calculated using the Gauge-Independent Atomic Orbital (GIAO) method, developed by Wolinski et al[33]. Polarizable Continuum Model (PCM) [34] through a single point (B3LYP/6-311+G(2d,p)) calculation[35] was employed to calculate the ^{1}H NMR chemical shift (DMSO-d_6 solvent: dielectric constant, ε = 46.826).

In order to check the sensitivity of the functional used two additional functionals (M06-2X and mPWB1W)[36, 37] was applied for geometric, IR and NMR calculations. These functionals have been reported to perform well for thermodynamics and kinetics[38, 39] in conjunction with larger 6-311++G(2d,2p) basis set[37]. Frequency calculations were performed with a scaling factor of 0.947[32]. All quantum chemical calculations have been performed using Gaussian 09 [40] software.

Natural Bond Orbital (NBO) analysis

Second-order perturbation theory is a vital tool used to study the delocalization of electron density. The NBO was calculated on DHAA-PH complexed with WT HIV-PR using at M06-2X /6-311++g(2d,2p). The electronic wave functions are described in terms of a set of unoccupied non-Lewis localised and molecular orbitals.[41] The conjugative (delocalisation) interaction was determined using the equation:

$$E^2 = \Delta E_{ij} = q_j \frac{F(i,j)^2}{\varepsilon_j - \varepsilon_i} \tag{1}$$

Where q_j is the donor orbital occupancy, ε_i and ε_j are diagonal matrix elements and $F(i,j)$ is the off-diagonal Fock matrix elements.

Molecular modelling
Molecular docking

The 3D crystal structure of WT-PR complexed with Ritonavir (PDB code: 1HXW)[3] was used as the starting structure. Docking studies were carried out using AutoDock tools [42] 1.5.4 software. The grid box which corresponds to the active site aspartate 25 (ASP 25) was (X= 15.938 Y= 26.981 Z= 4.533) and dimension (X=24 Y= 24 Z= 24) with 1.00 Å as the grid spacing employed. Gasteiger charges were computed using the AutoDock Tools graphical user interface supplied by MGL Tools [43]. The Lamarckian Genetic Algorithm, which regarded as one of the most reliable docking methods in Autodock[44, 45] was applied. The docked conformations of each compound were ranked based on their binding energies and binding pose. The docking procedure was tested with control using Ritonavir, which was docked into the active site of the enzyme and then compared to the crystal structure. DHAA-PH was aligned over the Ritonavir using Pymol software[46] (Fig. 2b)

Molecular dynamics simulations

The inhibitor-enzyme complex setup for Amber molecular dynamics was done in Antechamber tool implemented in Amber14[47]. The complex obtained from molecular docking was separated in Discovery studio software. The optimized ligand (DHAA-PH) was complexed with the enzyme in Amber. The complex was immersed in a cubic box with 10 Å distance of TIP3P[48] explicit water and counterions were added to neutralize the complex. The missing protons were treated using the X-leap[49] software. Molecular dynamics (MD) calculation were performed using Amber 14[50] package. MD simulations were carried out with the ff99SB[51] force field (for proteins) and GAFF[52] (DHAA-PH). Prior to MD simulations, two-stage geometric minimization was performed

by 2500 steps of steepest decent minimization followed by 2500 of conjugated gradient for relaxation of any steric clashes and contacts. First stage involves a minimization step with a constraint of 500 kcal/(mol·Å2). The second stage involved optimization without constraints. The system was then heated from 0 to 300 K under the NVT ensemble for 500 ps using the Langevin dynamics with a collision frequency of 1.0 ps^{-1}. All bonds involving hydrogen atoms were constrained using SHAKE algorithm[53]. Partial Mesh Ewald (PME)[54] method was applied to take care of long-range electrostatic interactions while with a cutoff of 12 Å was set for nonbonded van der Waals force. 1ns of protein-retrained equilibration MD with force constraint of 10 kcal/(mol·Å^2) was performed. 60 ns MD production with a time step of 2 fs with no harmonic restraints were run with the periodic boundary condition under the NPT ensemble at 300 K and a pressure of 1 atm. Analysis of RMSD was performed on Cα carbon of the protein backbone

Post MD analysis

MD trajectories analysis was performed for Root Mean Square Deviation (RMSD), Root Mean Square Fluctuation (RMSF) and radius of gyration (Rg) using PTRAJ and CPPTRAJ[55] in AMBER14.

MM-GBSA free energy calculations

The Binding free energies were computed using the MM-GBSA method in AMBER 14 package. A total number of 100 snapshots were chosen evenly from the last 2 ns on the MD trajectory, at an interval of 10 ps. The MM-GBSA method can be summarized as below:

$$\Delta G_{total} = G_{cpx} - \left(G_{rec} + G_{lig} \right) \tag{2}$$

where, the binding free energy, ΔG_{bind}, is estimated as follows:

$$\Delta G_{total} = \Delta E_{MM} + \Delta G_{sol} - T\Delta S \tag{3}$$

ΔG_{total} was measured as a sum of changes in the molecular mechanics (MM) gas-phase binding energy ΔE_{MM}, solvation energy ΔG_{sol} and entropy term (TΔS). The ΔE_{MM} was calculated by eqn 4.

$$\Delta E_{MM} = \Delta E_{int} + \Delta E_{vdw} + \Delta_{ele} \tag{4}$$

ΔE_{MM} is further divided into the amber force field internal energy terms (bond, angle and torsion), ΔE_{int}; the non-covalent van der Waals, ΔE_{vdw}; and electrostatic energies component, ΔE_{ele}.

In MM-GBSA method, the solvation free energy can be calculated as follows:

$$G_{sol} = G_{GB} + G_{nonpolar} \tag{5}$$

$$G_{nonpolar} = \gamma SASA + b \tag{6}$$

G_{GB} is taken as the polar solvation contribution calculated by solving the GB equation [24]

$G_{nonploar}$ is the non-polar salvation contribution, which was estimated by the solvent accessible surface area (SASA), which was determined using a water probe radius of 1.4 Å. The surface tension constant c was set to 0.0072 kcal/mol and b to 0 kcal/mol [56]

3D QSAR and ADMET study

All calculations of both target HIV1-protease inhibitory activity, ADMET and related properties such as toxicities, logP, pK$_a$, pK$_{ac}$ were performed using "Cinderella's Shoe" (CiS) and CoMIn software [57-60] considering both interior and exterior molecular characteristics on ChemoSophia web-portal [61][61][61][60][60]. The determination of pharmacophore, toxicophore fragments and the fragments responsible for metabolism were also performed using "Cinderella's Shoe" (CiS) and CoMIn software on ChemoSophia web-portal.

RESULTS AND DISCUSSION
Geometric properties

DFT predicted bond lengths, angles, dipole moment, bond angles, dipole moment and polarizability are presented in Table 1. DFT calculations gave good result and agreed with experiment. DFT calculations for C-C bond lengths (C1-C2) are close to experiment, but about 0.01-0.02 Å longer. Calculated O-C bonds are about 0.002 Å while calculated O1-C5 and N1-N2 is about 0.008 and 0.026 Å shorter than the experimental values. Calculated bond angles were also in agreement with the experimental values, though about 0.46 (°) slightly different. The good agreement observed may be because of the functional used and the basis set, since adding diffused and polarized functions enhance accuracy in (DFT) calculations. M06-2X and mPWB1W functional applied to improve the calculated geometries showed better correlation

Table 1: Selected bond distances (Å) and angles (•) for DHAA-PH obtained at B3LYP/6-31+G(d,p) levels of theory.

Bond lengths (Å)	B3LYP/6-31+G(d,p)	M06-2X/6-311++G(2d,2p)	mPWB1W/6-311++G(2d,2p)	Expt*
C1-C2	1.452	1.443	1.450	1.432
C2-C3	1.406	1.382	1.411	1.394
C3-C4	1.429	1.401	1.410	1.421
C4-C5	1.352	1.343	1.350	1.331
C10-C11	1.394	1.375	1.384	1.379
O1-C5	1.348	1.351	1.344	1.356
O2-C1	1.214	1.213	1.215	1.212
O3-C3	1.325	1.316	1.333	1.313
N1-N2	1.353	1.376	1.344	1.379
N1-C6	1.308	1.290	1.301	1.295
Bond angles (°)				
C(5)-O(1)-C(1)	123.92	123.30	123.88	123.46
C(6)-N(1)-N(2)	120.47	120.44	120.63	120.76
Single point calculation				
Dipole moment (D)	1.62	1.66	1.68	
Polarizability	60.35	60.43	6066	

Expt*: Experimental [16]

Table 2 . The experimental and calculated IR for DHAA-PH obtained using B3LYP/6-31+G(d,),
M06-2X/ 6-311++G(2d,2p) and mPWB1W/6-311++G(2d,2p).

Normal mode	Corrected calculated B3LYP/ 6-31G** harmonic frequency(cm⁻¹)	M06-2X	mPWB1W	Expt frequency (cm⁻¹)*	Assignment
ν_1	1,607	1,601	1,603	1,601	CH-N stretch
ν_2	1,677	1,683	1,686	1,684	C=O stretch
ν_3	3,052	3,054	3,058	3,055	C-H stretch
ν_4	3,410	3,301	3,340	3,300	N-H stretch
ν_5	3,466	3,421	3,455	3,455	O-H stretch

Expt*: Experimental frequency [16]. The experimental spectrum is presented in the supplementary material Figure S3

with experimental values. Polarizability α is the capacity for a molecule to be polarized. It is a property of matter; it controls the dynamical fields. Calculated dipole moment and polarizability was reported as 1.62 D and 60.4 Å³.

IR Spectra

The experimental IR spectra are shown in Fig. S3. A broad band was observed at 1,601 cm⁻¹ which were assigned to νCH-N band and this agrees with experimental data,

this is because of hydrogen bonding which is often strong in heterocyclic and amine substituted compounds. C=O, C-H, N-H bands were also strong and broad bands and are also in agreement with experimental data [16]. To evaluate the density functional used two other functionals, which has been reported to perform well with kinetics and thermodynamics was applied and the result showed that M06-2X and mPWB1W functional gave better agreement with experimental values.

Table 3: The experimental and calculated ^1H NMR and ^{13}C NMR chemical shift for DHAA-PH obtained using B3LYP 6-31+G(d,p) and M06-2X/6-311++G(2d,2p)

Nucleus	B3LYP/ 6-31G** in DMSO	M06-2X	Expt ^1H NMR (ppm)*	Nucleus	B3LYP/ 6-31G** in DMSO	Expt ^{13}C NMR (ppm)*
H3	2.10	2.16	2.18 (3H, s)	C19	16.22	15.90
H7	3.00	2.17	2.18 (3H, s)	C18	20.10	19.87
H8	2.17	2.17	2.18 (3H, s)	C3	93.34	96.26
H1	1.79	2.76	2.74 (3H, s)	C5	99.03	105.27
H4	1.10	2.74	2.74 (3H, s)	C16	105.29	113.40
H6	1.80	2.75	2.74 (3H, s)	C12	104.01	113.40
H9	8.21	5.81	5.81 (1H, s)	C14	110.84	122.07
H12	8.81	6.53	6.50 (1H, s)	C13	122.56	129.64
H5	6.91	6.81	6.88 (6H, m)	C15	120.93	129.64
H16	6.80	6.66	6.88 (6H, m)	C11	133.05	144.60
H14	7.26	7.31	7.33 (6H, Ar, m)	C2	158.20	163.12
				C6	162.40	168.65
				C4	163.30	180.40

Expt*: Experimental [16]. See Figure S2.

NMR spectra

Result in Table 3 revealed that some ^1H NMR chemical shift using B3LYP/6-31+G(d,p) functional was slightly overestimation which may be as a result of the underestimation the orbital energy inherent in the DFT method (B3LYP) [14]. The ^1H NMR signal at δ 2.17 (3H, s) is assigned to the methyl proton H_3C-C. The signals at δ 8.21 (1H, s) and 8.81 (1H, s) are assigned to methine protons, H-C. The signals at δ 6.91 (6H, m) and 6.80 (6H, m) are assigned to phenyl protons. Analysis of the ^1H NMR chemical shift using M06-2X/6-311++G(2d,2p) showed better correlation with experimental ^1H NMR signals with an average deviation of 0.01

Electronic properties

Frontier Molecular Orbital represented in the form of highest occupied molecular orbital (HOMO) and the lowest unoccupied molecular orbital (LUMO), is a central parameter that defines electron density [62-64] around a molecule and it also proposes the reactivity [63, 65] of the compound. The LUMO-HOMO (energy gap) of DHAA-PH was calculated to be 3.68 eV, this corresponds to π-π* transition a high reactivity. Using a more accurate functional and higher basis set, M06-2X/6-311++G(2d,2p) the HOMO-LUMO energy gap was observed to 3.41 eV

which is lower compared that observed for B3LYP functional. The LUMO is extended over the C-C bonds, the nitrogen and oxygen atom. The LUMO spreads over the entire molecule framework due to electron delocalization [66] while the HOMO is distributed over the C=C bonds (Fig. 1)

The calculated absorption data of DHAA-PH showed three distinct bands which were designated as S_0 to S_1, S_0 to S_2, S_0 to S_3 in increasing order of excitation energy (3.49 to 4.50 eV). The absorption wavelength (λ_{max}) arising from the S_0 to S_1 transition is 355.14 nm; this excitation corresponds to the HOMO-LUMO transition. This is a broad band with moderately high intensity (oscillator strength of 0.6) which implies that it is quantum mechanically allowed (allowed transition), suggesting a strong intramolecular charge transfer character [63, 67]. The absorptions λ_{max} arising from S_0 to S_2 and S_0 to S_3 transitions are 281.58 and 275.30 nm respectively. These excitations correspond to the promotion of an electron from HOMO-LUMO +1 and HOMO-LUMO +2 respectively. Because of their low intensity, it implies they are both quantum mechanically forbidden. The absorptions λ_{max} arising from S_0 to S_1, S_0 to S_2 transitions with M06-2X/6-311++G(2d,2p) were 354.2 and 322.5 nm respectively. The promotion of electrons from HOMO-
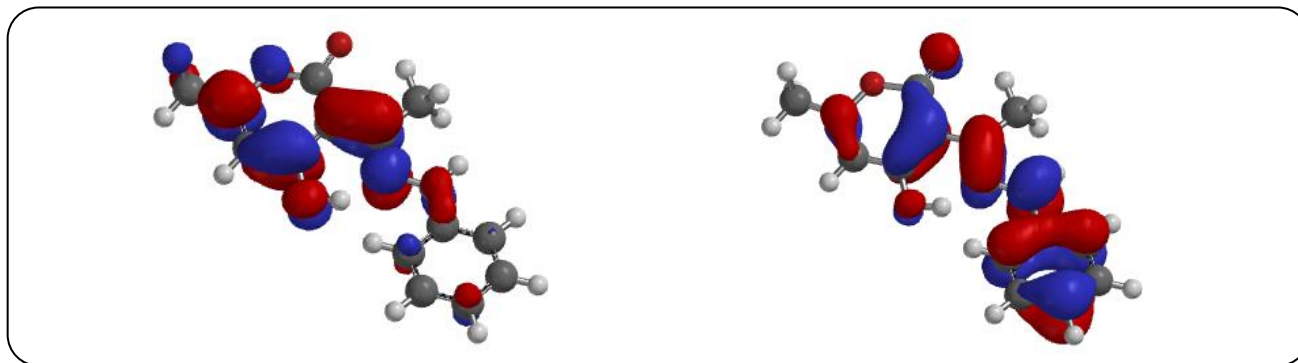
         Research Article

Fig. 1: LUMO and HOMO of DHAA-PH showing the distribution of electron density obtained at the DFT method.

LUMO+1 were observed to be a mechanically allowed transition. These properties are particularly useful for determining the relative strength of compounds in drug discovery.

Molecular docking

To explain and understand the biological and interaction potential of DHAA-PH, molecular docking approach has been done to determine the binding affinity with WT-PR to ascertain the interactions (Fig. 3a). Docking studies are essential in the prediction of ligand-receptor complex structures and to rank the ligand molecules according to the binding energies. The binding energies of the docked DHAA-PH based on the best three poses are presented in Table S4. The cage heteroatoms formed a strong hydrogen bonding interaction with the enzymatic aspartic acid (Asp25) residues. The carbonyl group hydrogen bonds with the side of the side chains of isoleucine (ILE50/ ILE50') and Glycine (GLY27) side chain formed a hydrophobic interaction with the N-H group of connecting the phenyl group (Fig. 3b). Fig. 4 also showed a good interaction between the compound and WT-PR. The molecular docking simulation clearly showed that the inhibitor fits into the active site of the enzyme pockets.

Flexibility and Stability indices (RMSF/RMSD)

The RMSD plot.[69-71] provides insight into the atomic fluctuations and structural movement from initial coordinates over MD tractories. 60 ns MD simulations were performed and to see the consistency of the simulation process, Root Mean Square Deviation (RMSD) of the DHAA-PH backbone was analysed and plotted as shown in Fig. 3.

The RMSD of DHAA-PH was stable within 1.0-2.0 Å, except for simulations of 30 ns and 40ns which had a high deviation but this normalized and became stable after 40ns. The trajectories thus became stable up to 60ns thus proving a suitable basis for further analyses.

Root mean square fluctuation (RMSF) of the Cα atoms were analyzed to give intuition into the fluctuation and flexibility of different regions of the amino acid residues[72, 73]. Fig. 4 indicates much higher fluctuations for the most part of the flap regions (residue 43-56 and residue 100-150).

The flexibility of the flap region is vital to the activity of the protease and flap dynamics of HIV-1 PR is related to the substrate binding and it plays a very important role in inhibitor effectiveness.[74] It was reported that these regions facilitate the entry and binding of a substrate/inhibitor in the active site through their movements. Even though this is not within the scope of this study, their fluctuations can circuitously lead to significant conformational changes in the active site cavity.

Binding free energy (ΔGbind) analysis

Calculated binding energies of DHAA-PH complexed with WT HIV-1-PR was determined using the MM-GBSA/PBSA method, by extracting 1000 snapshots at 10 ps interval from the last 10 ns production MD trajectories. The entropy (-TΔS) contributions were calculated using normal mode analysis [67, 68] by extracting 100 snapshots from the MD trajectories. The contributing binding components upon complexation, namely, ΔE_{vdw}, ΔE_{ele}, ΔG_{gas}, ΔG_{polar}, $\Delta G_{nonpolar}$ and $\Delta G_{solvation}$ are shown in Table 4. The results reveal binding free energies (ΔG_{bind}) of -22.9 kcal/mol which is higher and better than the reported
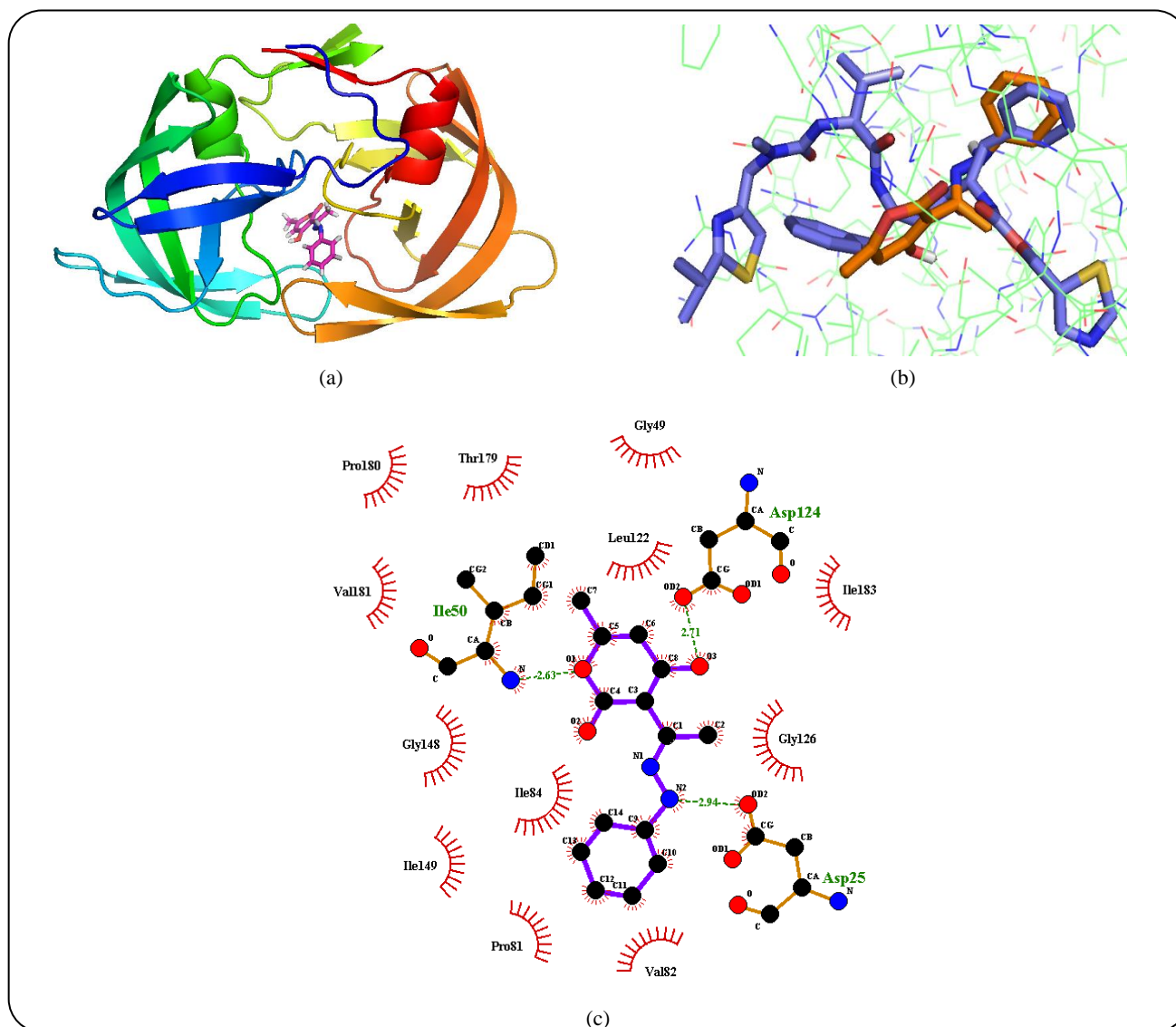
Fig. 2: (a) 3D diagram of DHAA-PH in complex with WT HIV-1-PR (b) Aligned docked pose with the control experiment
(b) hydrogen bond interactions for the WT HIV-PR complexes with DHAA-PH from the MD simulation. These plots
were created with the Ligplot software.[68]

experimental binding energies of wildtype C-SA HIV PR in complex with the FDA approved drugs[75]. The binding energies are characterised by a more negative van der Waals value and they are less electronegative. The estimation of the binding free in this study will provide valuable insight into the development of new HIV-1 protease inhibitors.

Natural bond orbital analysis (NBO)

Second order perturbation theory explains that large E^2 values demonstrate strong and intense molecular orbital interactions and charge transfer between donor and acceptor in a molecular system.[65, 76, 77]. Table 5 shows that stabilization energy E^2 for the transfer of electron from a lone pair (LP) of the O_{10} atom of the donor (Asp25 of WT HIV-1-PR) to the $\sigma^* N_{28}$—H_{29} of the acceptor indicating high intermolecular interaction (Fig. 5).

3D QSAR and ADMET analysis

The 3D QSAR study and the ADMET properties were performed at web-portal www.chemosophia.com [61][61][61][60][60] in the framework of the "Cinderella Shoe" method[58, 60], and also within the CoMIn algorithm[57, 59]. Results showed that DHAA-PH has

***Table 4: Calculated binding free energies and normal mode analysis DHAA-PH complexed with WT HIV-PR
obtained over the last 10 ns MD simulations. Energy components are in kcal/mol.***

Free energy method	Distribution	GBSA	PBSA
	ΔE_{vdw}	-28.6±3.3	-28.6±3.3
	ΔE_{elec}	-6.6±3.2	-6.6±3.2
	ΔG_{gas}	-35.3±4.4	-35.3±4.4
	ΔG_{sol}	12.5±3.0	37.1±7.3
	ΔG_{bind}	-22.9±3.5	-1.7±6.4
	$-T\Delta S$		
	ΔG_{expt} [a]	-13.9	

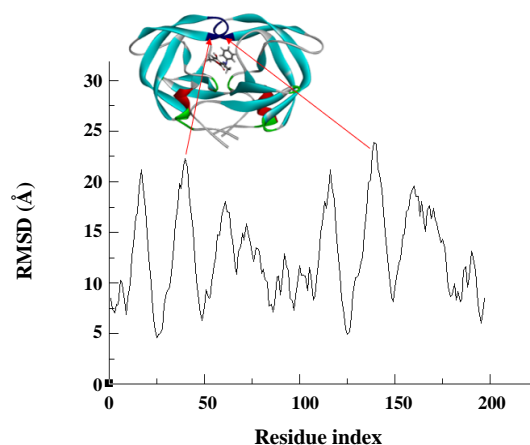ΔG_{bind} = Calculated ΔG binding Using MMGBSA/PBSA, Exp (ΔG)[a] = Experimental[75]
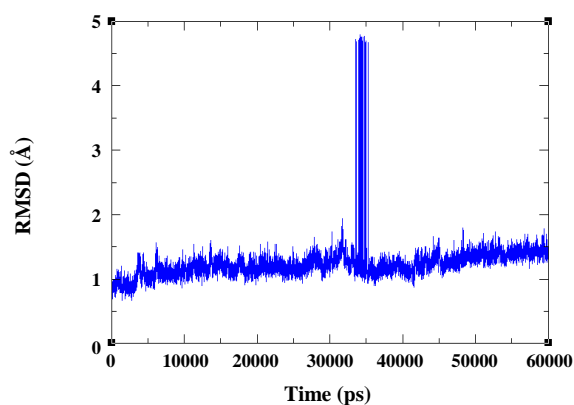
Fig. 3: The RMSD plot DHAA-PH complexed with WT HIV-PR obtained as a function of 60 ns MD runs.

Fig. 4: The per-residue RMSF of Cₐ atoms for DHAA-PH complexed with WT HIV-PR obtained as a function of 60 ns MD runs.

high inhibition activity against HIV-1 protease (see Table 1). The pharmacophore part of the DHAA-PH is localized on almost all peripheral atoms (red colour in Fig. 6) excluding carbonyl oxygen which does not contradict the results of molecular docking (Fig. 2c). The greatest contribution into anti-malarial activity is made by red-coloured atoms inside the red ellipse: hydrogen in 5 position, hydrogen of the 4-hydroxy group and the methyl hydrogens. According to the results of the docking, these fragments play the role of a spacer between Ile84 and Gly126.

A study of ADMET properties, showed that the logP value of DHAA-PH is 1.88 falls well in the range of Lipinski's rule of five[78, 79] and the probability of toxicity is high enough (the value is 0.8018). The toxicoforic parts of DHAA-PH are not unexpected.

These are sufficiently reactive pyrane oxygen, hydroxy substituent and hydrazonoyl group as it is shown in Fig. 7.

The probability of metabolism by cytochrome P450 3A4 isoform is high (0.9993) at 2D6 isoform is also high (0.5359) (Table 6). Most likely, in *in vivo* studies, the molecule will not reach the target due to metabolism. Metabolic vulnerabilities for CYP450 3A4 cover a significant portion of the molecule (Fig. 8), while the potential centers for metabolism by CYP450, 2D6 are only all oxygens and a nitrogen of hydrazonoyl group.

Furthermore, pK_a calculated was 7.95 and pK_a for conjugated acid (pK_{ca}) was 2.32 (i.e., the compound possesses low acidity and basicity) that also presuppose low undesirable effects.

Table 5: Second-order perturbation stabilization energies corresponding to the main intermolecular charge transfer interaction (Donor to Acceptor) between DHAA-PH and Asp25 of WT HIV-1-PR using M06-2X /6-311++g(2d,2p).

Donor	Acceptor	E^2 (kcal mol^{-1})
LP(O_{10})	σ^* (N_{28}—H_{29})	48.33
LP(O_{10})	σ^* (N_{28}—H_{29})	21.10
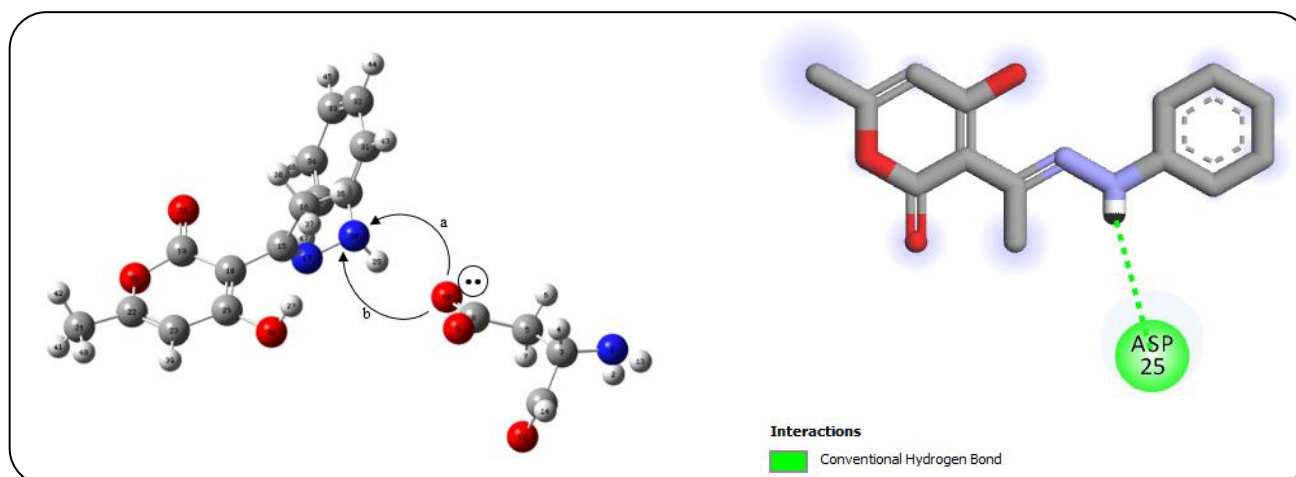
Fig. 5: (a) Description of intermolecular charge transfer obtained from Fock-matrix in NBO analysis. (b) 2D diagram showing the hydrogen bonding interaction between N-H of DHAA-PH and Asp25 of WT HIV-1-PR. The curved arrows (a and b) represents the direction of charge transfer from lone pair to antibonding (LP→ σ).*
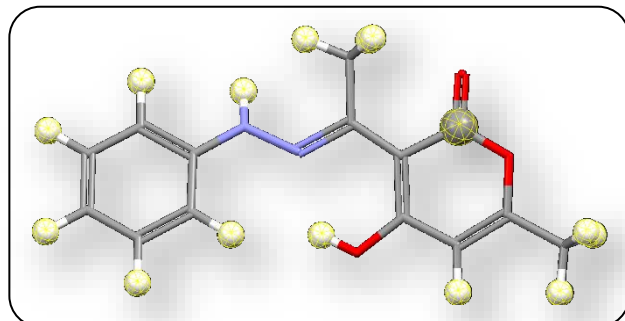
Fig. 6: Pharmacophore parts of the DHAA-PH (shown as balls) obtained using framework of the "Cinderella Shoe" method and within the CoMIn algorithm.
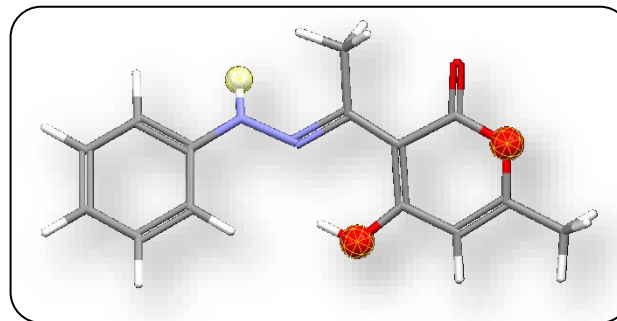
Fig. 7: Toxicophoric parts of DHAA-PH (shown as balls) obtained using framework of the "Cinderella Shoe" method and within the CoMIn algorithm.

Therefore, DHAA-PH can be a promising drug but the subsequent design of new HIV-1 protease inhibitors should include not only an increase in anti-HIV activity but also a decrease in toxicity and ability to metabolize. For this reason, changes could be made to the fragments responsible for toxicity and metabolism, without affecting the pharmacophoric fragments. The atoms that can be replaced to achieve above-mentioned goals are all oxygens and the anilide nitrogen. Obvious variants of changes

in the structure are the replacement of oxygens by sulfur and NH group by CH_2. The newly designed structures are represented in Scheme 2.

The computation of their characteristics shows the following (Table 1). The promising target anti-HIV1-protease inhibitory activity should have the compounds **III** and **IV**. Their logP values fit well into the Lipinski's rule of five. They should also have low acidity and basicity. Both compounds showed decreased metabolic activities

Table 6: Calculated probabilities of HIV1-protease inhibition (HIV1), ADMET properties such as probability of toxicity (Toxicity), probabilities of metabolism at isoforms CYP450 3A4 (CYP450 3A4) and CYP450 2D6 (CYP450 2D6), pK for acids (pK$_a$) and for conjugated acids (pK$_{ca}$).

Molecule	HIV-1	Toxicity	CYP450 3A4	CYP450 2D6	logP	pK$_a$	pK$_{ca}$
I	0.4882	0.7241	0.7712	0.0435	2.32	7.04	1.95
II	0.0762	0.8759	0.9978	0.9056	3.06	8.43	1.62
III	0.5852	0.9206	0.9986	0.4880	3.03	8.13	2.78
IV	0.8113	0.7011	0.9872	0.0137	1.90	8.76	3.69
DHAA-PH	0.5584	0.8018	0.9993	0.5359	1.88	7.95	2.32

(a)   (b)
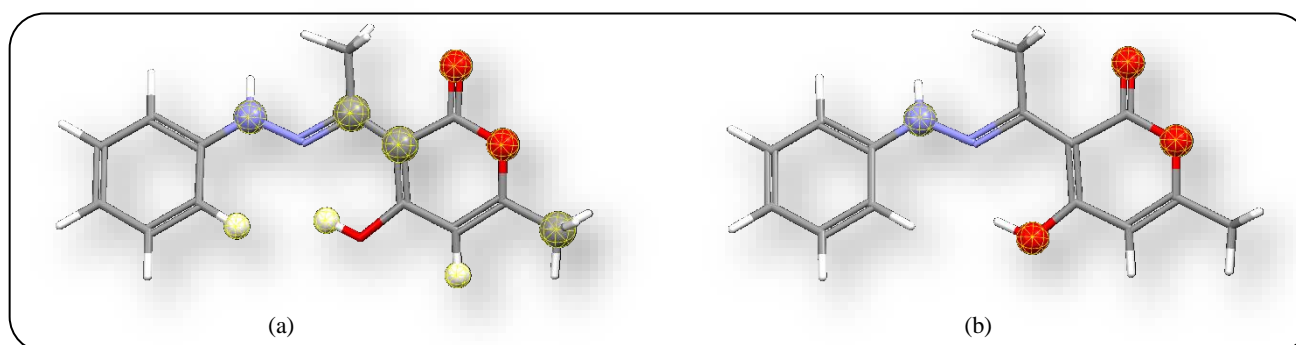
Fig. 8: Parts of DHAA-PH responsible for metabolism (shown as balls) by CYP450 a) 3A4; b) 2D6 isoforms.

I   **II**   **III**   **IV**
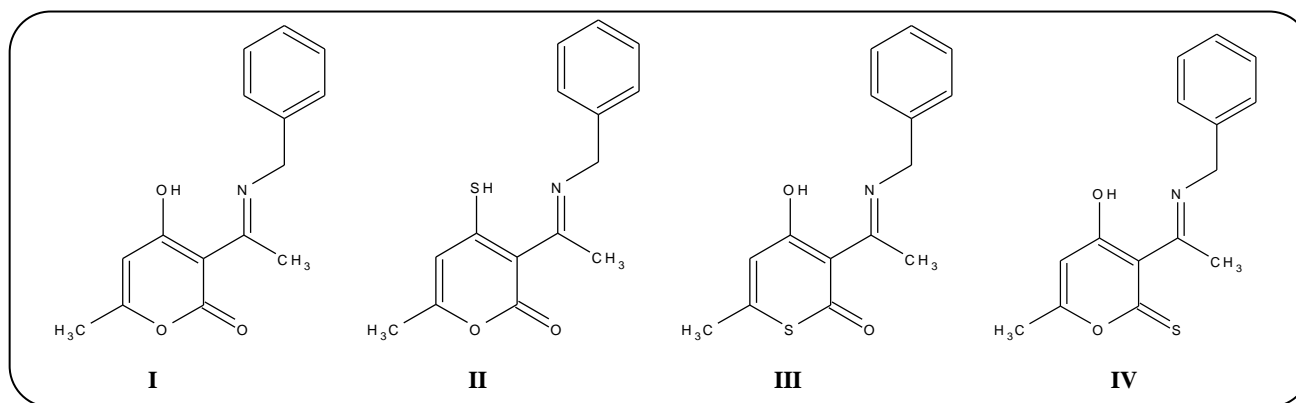
Scheme 2: The newly proposed structures with potential anti-HIV1-protease inhibitory activity.

relative to the parent compound DHAA-PH, however, the decrease in metabolic activity on the isoform CYP 3A4 is small enough and remains high. Moreover, the toxicity of compound **III** should increase relative to the parent compound DHAA-PH and, in this case, compound **IV** is the most promising among all newly designed compounds which possess improved target activity, toxicity and metabolic properties. The further way for the design of new promising anti-HIV1 drugs should include further improvement of metabolic properties with respect to isoform CYP 3A4.

CONCLUSIONS

MD and DFT simulation studies were carried out to understand inhibitor/enzyme interaction. DFT studies on DHAA-PH has been carried out using the hybrid Density Functional Theory (DFT) method at B3LYP/6-31G*, M06-2X/6-311++G(2d,2p) and mPWB1W/6-

311++G(2d,2p) levels of theory. The result showed that the studied inhibitor has good binding properties such as polarizability of 60.4 Å^3 and energy gap of 3.68 and 3.41 eV, which corresponds to π-π* electronic transition. M06-2X/6-311++G(2d,2p) and mPWB1W/6-311++G(2d,2p) showed better agreement with experimental values. Natural bond orbital analysis using the second perturbation energy E^2 obtained using M06-2X/6-311++G(2d,2p) revealed that DHAA-PH complex displayed stronger intermolecular charge transfer. The sides chain that formed good interactions and hydrogen bonding with the backbones of DHAA-PH are aspartic acid (Asp25), isoleucine (ILE50/ ILE50') and Glycine (GLY27). We hope this will facilitate the new drugs discovery for HIV treatments. A 3D QSAR and computational ADMET study of 4-hydroxy-6-methyl-3-[(1E)-1-(2-phenylhydrazinylidene) ethyl]-2H-pyran-2-one has been performed. Pharmacophore fragments of the compound have been identified as well as the fragments determining its toxicity and metabolic properties. Based on the analysis of these fragments, the ways to further design of promising HIV1-protease inhibitors have been proposed.

Acknowledgment

REFERENCES

[1] UNAIDs U., Organization W.H., Global HIV/AIDS Response: Epidemic Update and Health Sector Progress Towards Universal Access: Progress Report 2011, Global HIV/AIDS Response: Epidemic Update and Health Sector Progress Towards Universal Access: Progress Report (2011).

[2] Wlodawer A., Rational Approach to AIDS Drug Design Through Structural Biology, *Annu. Rev. Med (ARM)*, **53(1)**: 595-614 (2002).

[3] Sham H.L. Zhao, C., Stewart, K.D., Betebenner D.A., Lin S., Park C.H., Kong X.P., Rosenbrook W., Herrin T., Madigan D., A novel, Picomolar Inhibitor of Human Immunodeficiency Virus Type 1 Protease, *J. Med. Chem. (JMC)*, **39(2)**: 92-397 (1996).

[4] Honarparvar B., Makatini M.M., Pawar S.A., Petzold K., Soliman M.E., Arvidsson P.I., Sayed Y., Govender T., Maguire G.E., Kruger H.G., Pentacycloundecane-diol-Based HIV-1 Protease Inhibitors: Biological Screening, 2D NMR, and Molecular Simulation Studies, *Chem. Med. Chem (CMC)*, 7(6): 1009-1019 (2012.)

[5] Wlodawer A., Miller M., JASK6LsKi M., Sathyanarayana B.K., Baldwin E., Weber I.T., Selk L.M., Clawson L., Schneider J., Kent S.B., Crystal Structure of Synthetic HIV-Protease, *Science*, **245(4918)**: 6I6-621 (1989).

[6] Swain A.L., Miller M.M., Green J., Rich D.H., Schneider J., Kent S., Wlodawer A., X-Ray Crystallographic Structure of a Complex Between a Synthetic Protease of Human Immunodeficiency Virus 1 and a Substrate-Based Hydroxyethylamine Inhibitor, *Proceedings of the National Academy of Sciences (NAS)*, **87(22)**: 8805-8809 (1990).

[7] Prabu-Jeyabalan M.N.E., Schiffer C.A., Substrate Shape Determines Specificity of Recognition for HIV-1 Protease: Analysis of Crystal Structures of Six Substrate Complexes, *Structure*, **10(3)**: 369-381 (2002)

[8] Chen X., Tropsha,A., Relative Binding Free Energies of Peptide Inhibitors of HIV-1 Protease: the Influence of the Active Site Protonation State, *J. Med. Chem. (JMC)*, **38**(1): 42-48 (1995)

[9] Velazquez-Campoy A., Kiso Y., Freire E., The Binding Energetics of First-and Second-Generation HIV-1 Protease Inhibitors: Implications for Drug Design, *Arch. Biochem. Biophys. (ABB)*, **390**(2): 169-175 (2001)

[10] King N.M., Prabu-Jeyabalan M., Nalivaika E.A., Wigerinck P., de Béthune M.P., Schiffer C.A., Structural and Thermodynamic Basis for the Binding of TMC114, a Next-Generation Human Immunodeficiency Virus Type 1 Protease Inhibitor, *J. Virol. (JV)*, **78**(21): 12012-12021 (2004).

[11] McCoy C., Darunavir: a Nonpeptidic Antiretroviral Protease Inhibitor, *Clin Ther (CT)*, **29(8)**: 1559-1576 (2007).

[12] Woodard B.T., Posner G.H., Recent Advances in Diels-Alder Cycloadditions of 2-Pyrones, *Advances in Cycloaddition,* **5**: 47-84 (1999).

[13] Gupta A., Pal R., Beniwal V., Novel Dehydroacetic Acid Based Hydrazone Schiff's Base Metal Complexes of First Transition Series: Synthesis and Biological Evaluation Study, *World J. Pharm. Pharmaceut. Sci,* **4(1)**: 4990-1008 (2015).

[14] Prakash R.P., Kumar A., Singh S.P., Dehydroacetic Acid and Its Derivatives in Organic Synthesis: Synthesis of Some New 2-Substituted-4-(5-Bromo-4-Hydroxy-6-Methyl-2H-Pyran-2-One-3-Yl) Thiazoles, *Indian J. Chem*, (IJC), **46**: 1713-1715 (2007).

[15] Raman N., Thalamuthu S., Dhaveethuraja J., Neelakandan M., Banerjee S., DNA Cleavage and Antimicrobial Activity Studies on Transition Metal (II) Complexes of 4-Aminoantipyrine Derivative, *J. Chil Chem. Soc (JCCS),* **53(1)**: 1439-1443 (2008).

[16] Ujam O., Ogbonna O., Oliver A., Ume J., Janusson E., Chime C., Crystal Structure of 4-hydroxy-6-methyl-3-[(1E)-1-(2-phenylhydrazinylidene) ethyl]-2H-pyran-2-one, *Journal of Struct Chem, (SC)* **58(3)**: 636-639 (2017).

[17] Rosenfeld R., Vajda S., DeLisi C., Flexible Docking and Design, *Annu Rev Biophys Biomol Struct (ARBBS),* **24(1)**: 677-700 (1995).

[18] Holloway M.K., Wai J.M., Halgren T.A., Fitzgerald P.M., Vacca J.P., Dorsey B.D., Levin R.B., Thompson W.J., Chen L.J., A Priori Prediction of Activity for HIV-1 Protease Inhibitors Employing Energy Minimization in the Active Site, *J. Med. Chem (JMC)* **38**(2): 305-317 (1995).

[19] Caflisch A., Karplus M., Computational Combinatorial Chemistry for De Novo Ligand Design: Review and Assessment, *Perspectives in Drug Discovery and Design (PDDD),* **3**(**1**): 51-84 (1995).

[20] Roux B., Nina M., Pomès R., Smith J.C., Thermodynamic Stability of Water Molecules in the Bacteriorhodopsin Proton Channel: A Molecular Dynamics Free Energy Perturbation Study, *Biophys J. (BJ)* **71(2)**: 670-681 (1996).

[21] Briggs J.M., Marrone T.J., McCammon J.A., Computational Science New Horizons and Relevance to Pharmaceutical Design, *Trends Cardiovasc Med (TCM)* **6(6)**: 198-203 (1996).

[22] Srinivasan J., Cheatham T.E., Cieplak P., Kollman P.A., Case D.A., Continuum Solvent Studies of the Stability of DNA, RNA, and Phosphoramidate− DNA Helices, *J. Am. Chem. Soc (JACS),* **120(37)**: 9401-9409 (1998).

[23] Kollman P.A., Massova I., Reyes C., Kuhn B., Huo S., Chong L., Lee M., Lee T., Duan Y., Wang W., Calculating structures and Free Energies of Complex Molecules: Combining Molecular Mechanics and Continuum Models, A*cc. Chem. Res (ACR)*, **33(12)**: 889-897 (2000).

[24] Gourmala C., Luo Y., Barbault F., Zhang Y., Ghalem S., Maurel F., Fan B., Elucidation of the LewisX–LewisX carbohydrate Interaction With Molecular Dynamics Simulations: A Glycosynapse Model, *J. Molec. Struct: THEOCHEM,* **821(1)**: 22-29 (2007).

[25] Shaikh S.A., Jayaram B., A Swift All-Atom Energy-Based Computational Protocol to Predict DNA−Ligand Binding Affinity and ΔT_m, *J. Med. Chem* **50(9)**: 2240-2244 (2007).

[26] Gohlke H., Kiel C., Case D.A., Insights into Protein–Protein Binding by Binding Free Energy Calculation and Free Energy Decomposition For The Ras–Raf and Ras–Ralgds Complexes, *J. Mol. Biol (JMB),* **330(4)**: 891-913 (2003).

[27] Ode H., Matsuyama S., Hata M., Hoshino T., Kakizawa J., Sugiura W., Mechanism of Drug Resistance due to N88S in CRF01_AE HIV-1 Protease, Analyzed By Molecular Dynamics Simulations, *J. Med. Chem. (JMC)* **50(8)**: 1768-1777 (2007).

[28] Pandey P., Srivastava R., Bandyopadhyay P., Comparison of Molecular Mechanics-Poisson-Boltzmann Surface Area (MM-PBSA) and Molecular Mechanics-Three-Dimensional Reference Interaction Site Model (MM-3D-RISM) Method to Calculate the Binding Free Energy of Protein-Ligand Complexes: Effect of Metal Ion and Advance Statistical Test, *Chem. Phys. Lett* **695**: 69-78 (2018).

[29] Onufriev A., Bashford D., Case D.A., Exploring Protein Native States and Large-Scale Conformational Changes with a Modified Generalized Born Model, *Proteins: Structure, Function, and Bioinformatics* **55(2)**: 383-394 (2004).

[30] Hayashi S., Nakanishi W., Proposal for Sets of 77Se NMR Chemical Shifts in Planar and Perpendicular Orientations of Aryl Group and the Applications, Bioinorg. Chem. Appl. (2006).

[31] Lee C., Yang W., Parr R.G., Development of the Colle-Salvetti Correlation-Energy Formula into a Functional of the Electron Density, *Phys. Rev B,* **37(2)**: 785-789 (1988).

[32] Johnson R.D., NIST 101 Computational Chemistry Comparison and Benchmark Database (1999).

[33] Wolinski K., Hinton J.F., Pulay P., Efficient Implementation of the Gauge-Independent Atomic Orbital Method for NMR Chemical Shift Calculations, *J. Am. Chem. Soc. (JACS)* **112(23)**: 8251-8260 (1990).

[34] Cances E., Mennucci B., Tomasi J., A New Integral Equation Formalism for the Polarizable Continuum Model: Theoretical Background and Applications to Isotropic and Anisotropic Dielectrics, *J. Chem. Phys. (JCP)* **107(8)**: 3032-3041 (1997).

[35] De Souza L.A., Tavares W.M., Lopes A.P.M., Soeiro M.M., De Almeida W.B., Structural Analysis of Flavonoids In Solution Through DFT 1H NMR Chemical Shift Calculations: Epigallocatechin, Kaempferol and Quercetin, *Chem. Phys. Lett.,* **676**: 46-52 (2017)

[36] Patet R.E., Caratzoulas S., Vlachos D.G., Adsorption in Zeolites Using mechanically Embedded ONIOM Clusters, *Phys. Chem. Chem. Phys.,* **18(37)**: 26094-26106 (2016).

[37] Calixto A.R., Brás N.F., Fernandes P.A., Ramos M.J., Reaction Mechanism of Human Renin Studied by Quantum Mechanics/Molecular Mechanics (QM/MM) Calculations, *ACS Catal.,* **4(11)**: 3869-3876 (2014).

[38] Ibeji C.U., Tolufashe G.F., Ntombela T., Govender T., Maguire G.E., Lamichhane G., Kruger H.G., Honarparvar B., The Catalytic Role of Water in the Binding Site of L,D Transpeptidase 2 within Acylation Mechanism: A QM/MM (ONIOM) Modeling, *Tuberculosis* **113**: 222-230 (2018).

[39] Cao Y., Han S., Yu L., Qian H.,. Chen J.Z, MD And QM/MM Studies on Long-Chain L-Alpha-Hydroxy Acid Oxidase: Substrate Binding Features and Oxidation Mechanism, *J. Phys. Chem. B,* **118(20)**: 5406-17 (2014).

[40] Frisch M., Trucks G., Schlegel H.B., Scuseria G., Robb M., Cheeseman J., Scalmani G., Barone V., Mennucci B., Petersson G., Gaussian 09, Revision D. 01, Gaussian, Inc., Wallingford CT, (2009).

[41] Reed A.E, Curtiss L.A., Weinhold F., Intermolecular Interactions from a Natural Bond Orbital, Donor-Acceptor Viewpoint, *Chem. Rev.* **88(6)**: 899-926 (1988).

[42] Sanner M.F., Python: a Programming Language for Software Integration and Development, *J Mol Graph Model,* **17(1)**: 57-61 (1999).

[43] Morris G.M., Huey R., Lindstrom W., Sanner M.F., Belew R.K., Goodsell D.S., Olson A.J., AutoDock4 and AutoDockTools4: Automated docking with selective receptor flexibility, *J. Comput. Chem.* **30**(16): 2785-2791 (2009).

[44] Morris G.M., Goodsell D.S., Halliday R.S., Huey R., Hart W.E., Belew R.K., Olson A.J., Automated Docking Using a Lamarckian Genetic Algorithm and an Empirical Binding Free Energy Function, *J. Comput. Chem.* **19(14)**: 1639-1662 (1998).

[45] Huey R., Morris G.M., Olson A.J., Goodsell D.S., A Semiempirical Free Energy Force Field with Charge-Based Desolvation, *J. Comput. Chem.* **28(6)**: 1145-1152 (2007).

[46] Schrödinger L., PyMOL The PyMOL Molecular Graphics System, Version, (2010).

[47] Case D., Berryman J., Betz R., Cerutti D., Cheatham I., Darden T.A, Duke R.E, Giese T.J., Gohlke H., Goetz A.W., Homeyer N., Izadi S., Janowski P., Kaus J., Kovalenko A., Lee TS., LeGrand S., Li P., Luchko T., Luo R., Madej B., Merz K.M., Monard G., Needham P., Nguyen H., Nguyen H.T, Omelyan I., Onufriev A., Roe D.R, Roitberg A., Salomon-Ferrer R., Simmerling C.L., Smith W., Swails J., Walker R.C., Wang J., Wolf R.M., Wu X., York D.M., Kollman P.A., AMBER 14. 2014, University of California, San Francisco. (2015).

[48] Jorgensen W.L., Chandrasekhar J., Madura J.D., Impey R.W., Klein M.L., Comparison of Simple Potential Functions for Simulating Liquid Water, *J. Chem. Phys.,* **79(2)**: 926-935 (1983)

[49] Case D., Darden T., Cheatham III T., Simmerling C., Wang J., Duke R., Luo R., Crowley M., Walker R., Zhang W., AMBER, Version 10, University of California: San Francisco, CA (2008).

[50] Case D., Babin V., Berryman J., Betz R., Cai Q., Cerutti D., Cheatham III T., Darden T., Duke R., Gohlke H., AMBER 14. 2014, University of California, San Francisco (2014).

[51] Hornak V., Abel R., Okur A., Strockbine B., Roitberg A., Simmerling C., Comparison of Multiple Amber Force Fields and Development of Improved Protein Backbone Parameters, *PROTEINS*. **65**: 712-725 (2006).

[52] Wang J.M., Wolf, R.M., Caldwell J.W., Kollman P.A., Case, D.A., Development and Testing of a General Amber Force Field, *J. Comput Chem. (JCC),* **25:** 1157–1174 (2004).

[53] Ryckaert J.P., Ciccotti, G., Berendsen, H. J. C., Numerical Integration of the Cartesian Equations of Motion of A System with Constraints: Molecular Dynamics of N-Alkanes, *J. Comput. Phys. (JCP),* **23**: 327–341 (1977).

[54] Harvey F.G.D., An Implementation of the Smooth Particle Mesh Ewald Method on GPU Hardware, *J. Chem. Theory Comput* **5(9)**: 2371–2377 (2009).

[55] Roe D.R., Cheatham III T.E., PTRAJ and CPPTRAJ: Software for Processing and Analysis of Molecular Dynamics Trajectory Data, *J. Chem. Theory Comput* **9**(7) 3084-3095 (2013).

[56] Sitkoff D., Sharp K.A., Honig B., Accurate Calculation of Hydration Free Energies Using Macroscopic Solvent Models, *J. Phys. Chem.* **98**(7) 1978-1988 (1994).

[57] Potemkin A.V., Grishina M.A., Potemkin V.A., Grid-Based Continual Analysis of Molecular Interior for Drug Discovery, QSAR and QSPR, *Curr. Drug. Discov. Technol.* **14**(3): 181-205 (2017).

[58] Potemkin V., Grishina M., Principles for 3D/4D QSAR Classification of Drugs, *Drug discovery today* **13**(21-22): 952-959 (2008).

[59] Potemkin V., Grishina M., Grid-Based Technologies for In Silico Screening and Drug Design, *Curr. Med. Chem.* **25**(29): 3526-3537 (2018).

[60] Potemkin V., L. 21: Cinderella's Shoe for Virtual Drug Discovery Screening and Design, *Drugs of the Future* **35**: 14 (2010).

[61] Chemosophia s.r.o., Prague, https://vestnik.susu.ru/chemistry/article/view/7213. Accessed 16 (2018).

[62] Fakhar Z., Govender T., Lamichhane G., Maguire G.M.E., Kruger H.G., Honarparvar B., Computational Model for the Acylation Step of the B-Lactam Ring: Potential Application for L,D-Transpeptidase 2 in Mycobacterium Tuberculosis, *J. Mol. Struct*. **1128**: 94-102 (2017).

[63] Ibeji C.U., Adejoro I.A., Adeleke B.B., A Benchmark Study on the Properties of Unsubstituted and Some Substituted Polypyrroles, *J. Phys. Chem. B,* **5**(6): 2161- 0398 (2015).

[64] Ekennia A.C., Osowole A.A., Olasunkanmi L.O., Onwudiwe D.C., Olubiyi O.O., Ebenso E.E., Synthesis, Characterization, DFT Calculations and Molecular Docking Studies of Metal (II) Complexes, *J. Mol. Struct* **1150**: 279-292 (2017).

[65] Rauf S.M.A., Arvidsson P.I., Albericio F., Govender T., Maguire G.E., Kruger H.G., Honarparvar B., The Effect of N-Methylation of Amino Acids (Ac-X-Ome) on Solubility and Conformation: A DFT Study, *Org Biomol. Chem.* **13(39)**: 9993-10006 (2015).

[66] Lawal M.M., Govender T., Maguire G.E., Kruger H.G., Honarparvar B., DFT Study of the Acid-Catalyzed Esterification Reaction Mechanism of Methanol with Carboxylic Acid and Its Halide Derivatives, *Int. J. Quantum Chem.* **118(4)**: 25497 (2017).

[67] Kazaoui S., Minami N., Tanabe Y., ByrneH.J., Eilmes A., Petelenz P., Comprehensive Analysis of Intermolecular Charge-Transfer Excited States in C 60 and C 70 Films, *Phys. Rev*. B **58(12)**: 7689-(1998).

[68] Wallace A.C., Laskowski R.A., Thornton J.M., LIGPLOT: A Program to Generate Schematic Diagrams of Protein-Ligand Interactions, *Protein Eng*. **8(2)**: 127-134 (1995).

[69] Duan X., Zhang M., Zhang X., Wang F., Lei M., Molecular Modeling and Docking Study on Dopamine D2-Like and Serotonin 5-HT2A Receptors, *J. Mol. Graph. Model.* **57**: 143–155 (2015).

[70] Martinez L., Automatic Identification of Mobile and Rigid Substructures in Molecular Dynamics Simulations and Fractional Structural Fluctuation Analysis, *Plos One,* **10(3)**: e0119264 (2015).

[71] Kumalo H,M., Soliman M.E., Per-Residue Energy Footprints-Based Pharmacophore Modeling as an Enhanced In Silico Approach in Drug Discovery: A Case Study on the Identification of Novel β-Secretase1 (BACE1) Inhibitors as Anti-Alzheimer Agents, *Cell Mol.Bioeng.,* **9(1)**: 175-189 (2016).

[72] Minkara M.S., Ucisik M.N., Weaver M.N., Merz K.M., Molecular Dynamics Study of Helicobacter Pylori Urease, *J. Chem. Theory Comput.* **10(5)**: 1852-1862 (2014).

[73] Arodola O.A., Soliman M.E., Molecular Dynamics Simulations of Ligand-Induced Flap Conformational Changes in Cathepsin-D-A Comparative Study, *J. Cell. Biochem.* **117(11)**: 2643-2657 (2016).

[74] Chen J., Liang Z., Wang W., Yi C., Zhang S., Zhang Q., Revealing Origin of Decrease in Potency of Darunavir and Amprenavir Against HIV-2 Relative to HIV-1 Protease by Molecular Dynamics Simulations, *Scientific Reports* **4**: 6872 (2014).

[75] Maseko S.B., Padayachee E., Govender T., Sayed Y., Kruger G., Maguire G.E., Lin J., I36T↑ T Mutation in South African Subtype C (C-SA) HIV-1 Protease Significantly Alters Protease-Drug Interactions, *J. Biol. Chem.* **398(10)**: 1109-1117 (2017).

[76] Martins-Costa M., Anglada J.M., Ruiz-López M.F., Hyperconjugation in Adjacent OO Bonds: Remarkable Odd/Even Effects, *Chem. Phys. Lett.* **481**(4): 180-182 (2009).

[77] Greenway K.T., Bischoff A.G., Pinto B.M., Probing Hyperconjugation Experimentally with the Conformational Deuterium Isotope Effect, *J. Org. Chem.* **77(20)**: 9221-9226 (2012).

[78] Lipinski C.A., Lombardo F., Dominy B.W., Feeney P.J., Experimental and Computational Approaches to Estimate Solubility and Permeability in Drug Discovery and Development Settings, *Adv. Drug Deliv. Rev.* **23(1-3)**: 3-25 (1997).

[79] Lipinski C.A., Lead-and Drug-like compounds: The Rule-of-Five Revolution, *Drug Discov. Today: Technol.* **1(4)**: 337-341 (2004).